Experimental investigation of different nozzle designs inside active chilled beams

Max Rohn[1,*], *Paul* Mathis[1], *Dirk* Müller[1]

[1]RWTH Aachen University, E.ON Energy Research Center, Institute for Energy Efficient Buildings and Indoor Climate

Abstract. The aim of this study is to improve the performance of active chilled beams (ACB) by varying the nozzles cross section geometry. Most of the common ACB today have circular nozzles for the primary air plenum, as they are easy to produce and ensure a good performance. The amount of induced secondary air and thereby the performance of the system can be increased by improving the properties of the primary air jet. In other research fields like engine jets or air diffusers, different nozzle designs have been developed to enhance the jets mixing. In this study, a generic test bench is built to investigate different nozzle designs for ACB. The flow field is investigated with particle image velocimetry (PIV) which gives detailed information about the jet's shape. The designed test bench ensures optical access to the flow field while the induced room air is measured via differential pressure methods. The cross-shaped nozzle achieved the best results among the investigated ones and could significantly increase the induced air amount. An elliptic opening also shows promising results but cannot reach the performance of the circular nozzle in this study. A rectangular nozzle opening turns out to be unsuitable in ACB.

1 Introduction

The use of active chilled beams (ACB) in modern HVAC systems is receiving more attention during the last past years. Their significant advantages compared to typical all-air systems make them a promising opportunity regarding energy savings in the building sector. One major aspect is the reduction of the fresh air amount, which is proved in the studies of Mathis et al. [1]. In all-air systems the occurring heat loads are removed by supplying conditioned air, in the following called primary air, to the room. Due to the air's low heat capacity, the amount of air and thereby the energy consumption for conditioning and ventilation can be significant. In an ACB the amount of primary air is far smaller and delivered through multiple nozzles. Air from inside the room is induced by the emerging air jets and passes a heat exchanger, before mixing with the fresh air and being supplied to the room again (Fig. 1). Due to the better heat transfer conditions and the higher heat capacity of water, less space and energy is used for transporting the cooling medium. The ratio of induced room air and primary air is called induction ratio (IR). It is a suitable indicator for the performance of the system and its enhancement is one major goal when optimizing ACB. In the literature, different approaches to increase the IR can be found. The study by Guan and Wen [2] focuses on the geometric parameters of the ACB. By changing the fresh air plenum's geometry, the IR is highly affected. Smaller nozzle diameters and larger distances between the nozzles lead to an increase of the IR, whereas these changes also lead to smaller volume flows, which is not always acceptable because of the humidity restrictions inside the room.

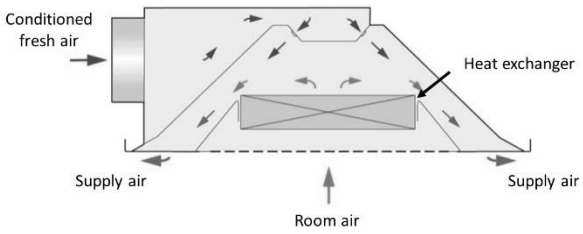

Fig. 1 Principle of an active chilled beam

High volume flows in the constellation small nozzle diameter and large distance between the nozzles [2], would lead to high pressure losses and high acoustic emission due to the high Reynolds numbers. A different change in geometry is presented in the studies by Freitag et al. [3]. In a generic ACB geometry, the entrainment area of the air jet, i.e. the area where the jet is not limited by walls and induces air, is changed. Enlarging this area results in higher IR. It is also shown that slightly enlarging the cross section of the air duct has a positive effect on the IR. Another approach is to reduce the airside pressure drop of the heat exchanger [3]. As this decision is in most cases a trade-off between pressure drop and effective heat transfer, it is usually not a considerable choice. Besides ACB there are several other research fields investigating free air jets. For example in aero engineering regarding the airplane's propulsion jet, the fuel jet in combustion

* Corresponding author: max.rohn@eonerc.rwth-aachen.de

engines or air supply diffusers for HVAC systems. Most of these researches have different intentions, like reducing the acoustic emission or enhancing the mixing with the ambient air. To reach these goals, many of them focus on the nozzle's cross section shape. Switching the shape from circular to rectangular for example, enhances the jet's mixing with ambient air because of counter-rotating streamwise vortices [4]. An elliptic nozzle geometry also has a slightly positive effect on the jet's mixing characteristics [5] and for a perforated diffuser an improvement regarding the self-induction was shown for cross-shaped nozzles [6]. This means more surrounding air is engulfed into the jet. In recent studies the cross-shaped nozzles have been expanded to lobed, i.e. overlapping cross-shaped nozzles, for further increased mixing [7].

In the first step, this study focusses on two-dimensional nozzle shapes, which is a slight simplification regarding the common ACB. Due to financial reasons, nozzles are produced by stamping metal sheets, so that usually a rounding at the nozzle entrance is produced. The aim of this study is to apply the previously described results of different nozzle shapes from other research areas to ACB. In an ACB, the flow velocities are much lower than in aero engine applications but higher compared to air diffusers. A certain momentum is necessary to induce the air from the room and to overcome the pressure losses inside the heat exchanger. This is in contrast to the high velocity decay that can be observed for the better mixing processes [3, 4, 5, 6]. For an ACB, the best choice is a trade-off between high mixing and a sufficient momentum. Moreover, in ACB the jets are simultaneously characterized as wall jets on the one hand and as free jets on the other hand. The plane facing towards the heat exchanger is not limited and therefore defined as free jet, whereas the opposing side of the jet is limited by a wall. Due to the Coanda effect and the momentum by the entrained room air, the jet is distracted and attaches to the wall. These reasons motivate to investigate the nozzle geometries inside an ACB separately.

2 Experimental setup

The four different nozzle geometries that are investigated are shown in Fig. 2.

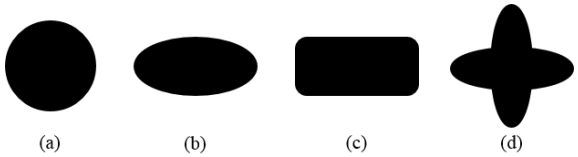

Fig. 2. Nozzle geometries

The reference case is the standard circular cross section (a), which is used in most of the ACB today. This case is compared to the different geometries found in the literature: Elliptic (b), rectangular (c) and cross-shaped (d). All geometries are milled into a metal sheet of 1 mm thickness. The difference compared to stamping the geometries is that no rounding is produced. Nevertheless, this study only considers two-dimensional aspects of the nozzle cross section, so that the rounding due to the manufacturing process is neglected. The nozzles' cross section area is constant for all geometries and all the measurement parameters are presented as multiples of the circle diameter D ($D_{circle} = 8\,mm$). A schematic illustration of the test bench is shown in Fig. 3. The opening underneath the nozzle imitates the opening towards the heat exchanger inside an ACB. Through this opening, the ambient room air enters the ACB and mixes with the conditioned primary air. For measuring the induced secondary air and thus the IR, the opening is fully covered with a hood (9). In the middle of the hood a package of different flow straighteners (4, 5) is installed to guarantee a homogeneous flow field. Inside the volume (3) between these applications and the duct, the differential pressure compared to the ambient air $\Delta p = p_3 - p_{amb}$ is measured with a differential pressure sensor (Sensirion SDP1000-L025). By controlling the radial fan for secondary air, Δp is kept at a value of 0 Pa. At this point, the supplied secondary airflow by the fan exactly corresponds to the induced airflow by the primary air jet in the undisturbed case. This airflow can be determined with the differential pressure method and an ISO 5167 standard orifice (6). The primary air is also supplied with a radial fan and determined by differential pressure methods. To ensure a comparability of the measurements, the Reynolds number based on the equivalent diameter of

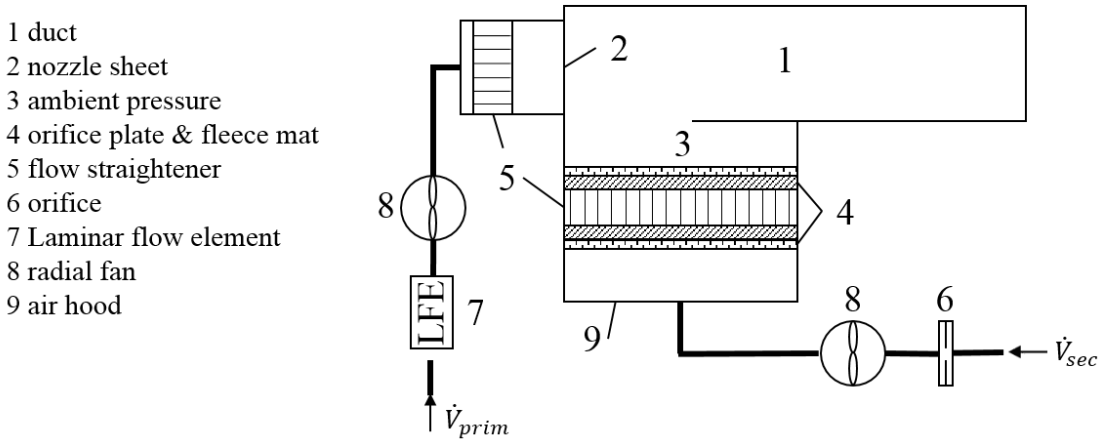

Fig. 3 Schematic of the test bench

a circular cross section is kept on a constant value of $Re_D = 5000$. As the airflow is small compared to the secondary airflow, the orifice is replaced by a laminar flow element (7), which is more suitable for small flow rates. To get information regarding the pressure loss of the different nozzle geometries, another pressure measurement is installed between the flow straightener (5) and the nozzle sheet (2). The necessary pressure to ensure this Reynolds number gives information about the pressure loss of each geometry. All values are recorded and controlled with an ET-87Pn control unit which is operated with a customized LABVIEW™ software. Fig. 4 shows the geometric parameters and the PIV system installation. The nozzle opening is centred on a square sheet with the width $W = 20D$ and the height $H = 20D$. The opening length is also $L = 20D$. The laser head is mounted above the duct and the camera positioned in a 90° angle to the laser plane. The corresponding walls of the duct are built of window glass to ensure optical access. As the installed PIV system is a two-dimensional, two component (2D2C) system, only two-dimensional velocity vectors in the x-y plane are recorded. To get information about the three-dimensional characteristics of the jet, the measurement plane is moved in z direction. The z-displacements are multiples of D referred to the centreline of the nozzle ($0D$).

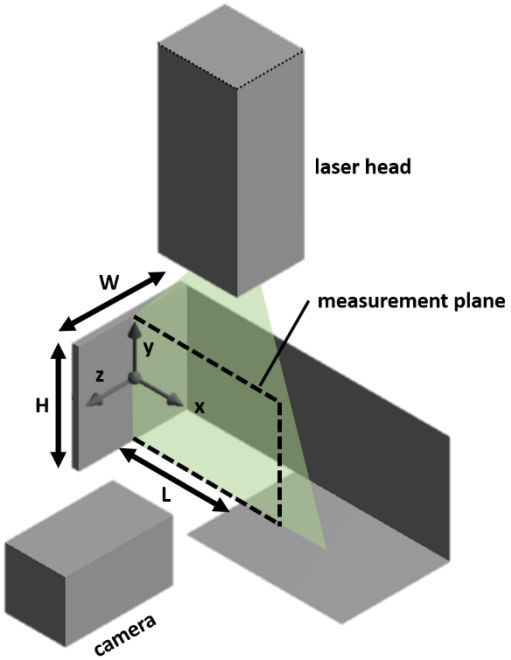

Fig. 4. PIV System and geometric parameters

To measure the flow field, liquid DEHS is nebulized in an aerosol generator (Palas AGK2000) and seeded into the flow as tracer particles. The particles are illuminated with a pulsed Nd:YAG laser (Quantel EverGreen 200) and the scattered light is recorded by a 5.5 MPixel sCMOS camera (HiSense Neo). Both components are synchronized with a BNC Model 575 synchronizing unit. The PIV system is operated with the software Dynamic Studio 4.0. The generated data is also post-processed with the software and graphical edited with the software ANSYS CFD-Post, Release 19.2. In terms of the post-processing some errors due to bright reflection or perspective distortion are minimized. The velocity vectors are calculated with the adaptive PIV method, which allows an automatic and adaptive calculation based on the particle images. Depending on the desired results, the software is also suitable to create mean velocity fields.

3 Results and discussion

Table 1 presents the measured induction ratio (IR) and the necessary plenum pressure to reach the required Reynolds number for the different nozzle cross sections. The cross-shaped nozzle increases the IR by 15.5 % and does not significantly affect the pressure loss compared to the reference case. By installing the elliptic nozzle, the pressure loss is slightly decreased but also the IR decreases by 3.0 %. For the rectangular cross section the IR is decreased by 8.3 % and therefore the worst result in this study. An advantage of the rectangular cross section is the low pressure loss. Because the energy consumption of an HVAC system is dependent on the supply pressure, the cases could also be compared at a constant plenum pressure. In that case, the IR for the rectangular and elliptic cross section would probably increase due to the higher Reynolds numbers.

Table 1. Induction Ratio and plenum pressure

	IR	**p [Pa]**
circular	8.4	80
cross-shaped	9.7	79
rectangular	7.7	75
elliptic	8.2	78

The reasons for these IR can be determined by analysing the generated PIV data. In Fig. 5 the mean velocity plot of the cross-shaped nozzle is shown.

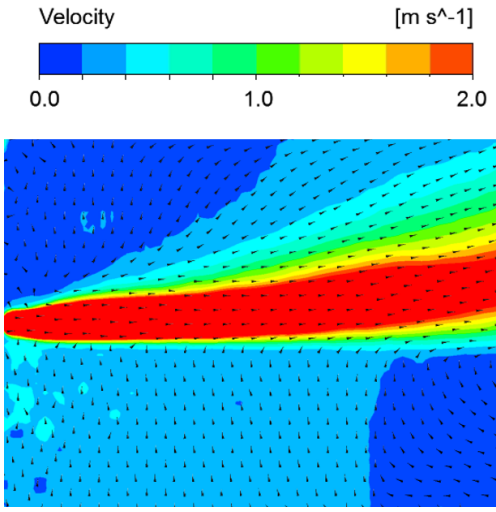

Fig. 5. Velocity plot of the cross-shaped nozzle

Arrowheads indicate the stream direction and the plotted data range is chosen to point out the small velocities of the induced secondary air. The plot shows how the jet widens due to the entrained surrounding air and how secondary air is induced from the opening. It is also clearly visible how the jet is distracted towards the top wall, which is caused by a combination of the secondary air's momentum from below and the Coanda effect that can be observed close to the top wall.

For a quantitative investigation, the velocity profiles of the different nozzle geometries are compared. The velocity component u in x-direction and its streamwise development are shown in the following figures. This profile is important to assess the momentum of the jet. By increasing the jet's flow velocity, the momentum of the jet into the duct and the turbulence intensity at the jet's edges is increased. Both are crucial parameters to induce secondary air from the opening. Fig. 6 and Fig. 7 show the velocity profiles at a streamwise distance of $x/D = 1$.

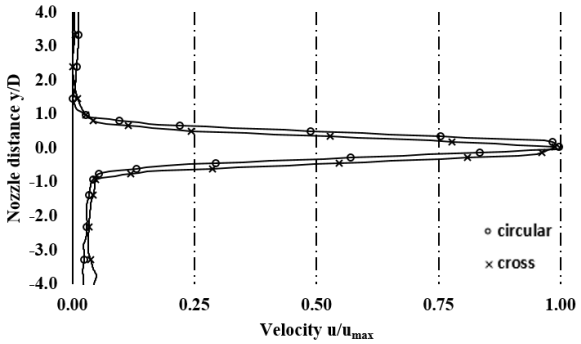

Fig. 6. Velocity profile u at *x/D*=1 for circular and cross-shaped cross section

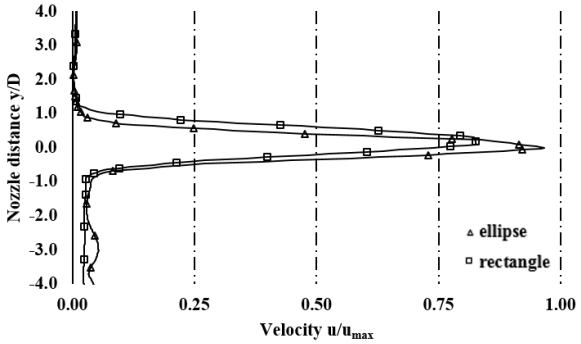

Fig. 7. Velocity profile u at *x/D*=1 for elliptic and rectangular cross section

The y-coordinate is normalized with the diameter D and the velocity u is normalized with the highest existing velocity u_{max}, which is found in front of the circular round nozzle. The velocity profile of the cross-shaped cross section is similar compared to the circular cross section and also the maximum velocity only differs slightly (Fig. 6). Fig. 7 shows that the maximum velocity for the elliptic cross section is about 4.0 % lower compared to the circular cross section. The jet from the rectangular nozzle cross section, creates the smallest momentum with a maximum velocity of 83.0 % of the circular jet. The measured profiles seem reasonable due to the constant Reynolds number. For a circular cross section a symmetric profile with high velocities in the centre develops. Regarding the rectangular cross section, the peak velocity is also found in the centre but unlike with the circular cross section the geometry is constant in z-direction for a certain distance. Thus, the velocity only decreases slowly in this direction. The result is a lower but wider peak velocity profile for the rectangular cross section. This explanation is underlined by Fig. 8, which shows the velocity profiles at the same distance $x/D = 1$ but at a z-displacement of $z/D = 0.5$. The circular profile is flat whereas the profile for the rectangular cross section is still present and the peak velocity reaches 13.0 % of u_{max}. The elliptic and cross profile at this plane are between the two profiles shown in Fig. 8. The elliptic profile amounts to 5.0 % and the cross profile to 7.0 % of u_{max} at this plane.

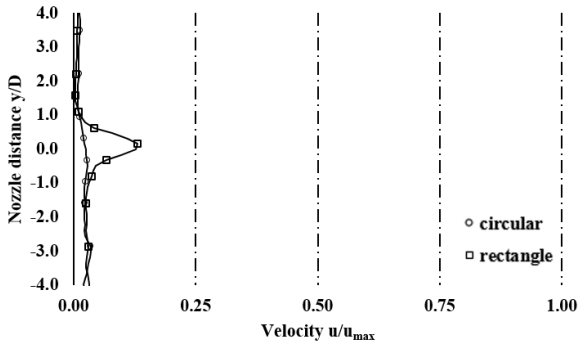

Fig. 8. Velocity profile u at x/D=1 and z/D=0.5 for circular and rectangular cross section

Regarding the IR, high jet velocities are advantageous. The peak velocities of the circular cross section are superior compared to the others, whereas the rectangular cross section creates a wider range of the velocity profile. The elliptic and cross-shaped cross section seem to be a good trade-off. Nevertheless, the jet velocity of the rectangular cross section, in the $z/D = 0.5$ plane, is only superior in the near field of the nozzle. In Fig. 9 the velocity fields in the same plane are plotted for a streamwise distance of $x/D = 10$. The rectangular jet has the lowest peak velocity and the circular jet, in contrast to the $z/D = 0$ plane, amounts to 88.0 % of the elliptic jet speed. It is shown that a certain core speed is required to maintain the initial advantage of speed in the outer regions. The cross jet is not shown because of clarity reasons but fits the elliptic jet well.

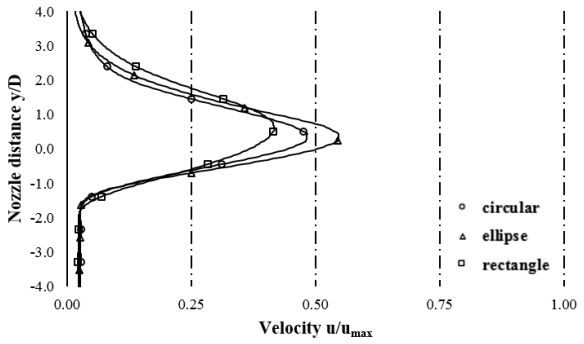

Fig. 9. Velocity profile *u* at *x/D*=10 and *z/D*=0.5 for circular, elliptic and rectangular opening

As a next step, the development of the profiles along the *x*-axis is investigated. The opening has a length of $20\,D$ and the whole distance can be used to induce secondary air. Fig. 10 shows the velocity profiles for all geometries at the end of the secondary opening (*x/D*=20). Due to the induced air from below and the Coanda effect, the jet is distracted towards the top of the duct. The velocity peak is now at a height of $y/D = 1.5$. The jet has already induced ambient air, which causes the bell-shaped velocity profile at this stage. The rectangular profile has still the lowest flow velocities with 22.0 % of u_{max}, which means a reduction of 73.3 % compared to the profile at *x/D*=1. The peak velocity for the circular profile is also decreased by 74.2 % and is now lower than for the cross and elliptic cross section. Their peak velocities are decreased by 72.0 % and 69.6 %, respectively.

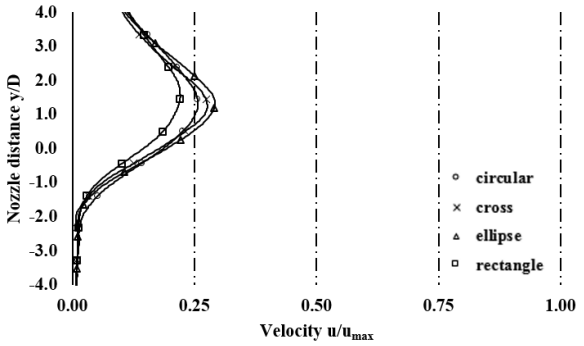

Fig. 10. Velocity profile *u* at *x/D*=20 for all geometries

So far, every geometry has shown some advantages. The circular nozzle cross section leads to high peak velocities at the entrance, whereas the rectangular cross section has a wider profile. The elliptic cross section seems to have a more stable streamwise flow field and the cross-shaped nozzle appears to be a good trade-off in all cases.

To get more information about how these aspects influence the induced flow field, the velocity fields above the opening are investigated. Fig. 11 shows the velocity component v in *y*-direction at a distance of $1\,D$ above the secondary opening at $z/D = 0$. The velocity is normalized with the maximum measured velocity v_{max} and the distance from the nozzle sheet is shown as multiples of *D*. Corresponding to Fig. 6 and Fig. 7, the elliptic and rectangular nozzle cross section generate the lowest flow velocities from the secondary opening. The cross-shaped nozzle cross section is superior to all the other geometries and generates the highest velocities, which are in average 13 % higher than for the circular cross section.

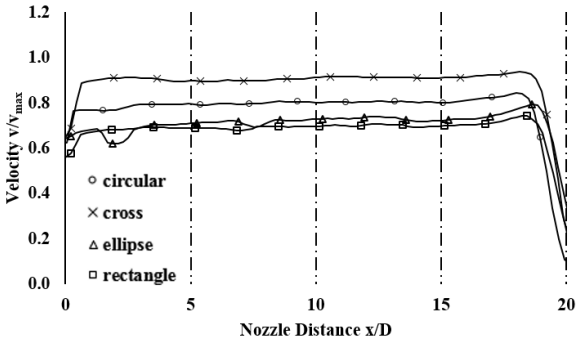

Fig. 11. Velocity profile *v* at *z/D*=0 for all geometries

As the velocity profile in Fig. 6 has shown slightly higher velocities for the circular opening, other effects besides the jet velocity need to be taken into account, to explain the induced velocity field. When the jet enters the duct, turbulent flow structures develop inside the shear layer and ensure the fluid exchange between the ambience and the jet. Concluding, a higher turbulence and vorticity generation of the nozzle geometry lead to a higher amount of induced air and thus to higher velocities in *y*-direction, respectively. The high velocities for the cross-shaped geometry in Fig. 11 indicate that the vorticity generation in this case is higher compared to the other cases. Vortices are transient and three-dimensional phenomena, thus hard to measure by the two-dimensional setup in this study. A good indicator for the vorticity strength inside the flow is the Q-criterion, which describes the second invariant of the velocity gradient tensor and is a measure of the rotation strength of the flow apart from rotation due to wall shear. Detailed information can be found in [8]. Fig. 12 shows the Q-criterion determined in the region between the jet and the secondary opening for the different geometries at $z/D = 0$. The qualitative plot shows, that the cross-shaped nozzle leads to higher vorticity of the flow inside the duct. There are more regions with high values for Q compared to the circular or rectangular cross section. For the elliptic cross section the vorticity is also enhanced, but still below the values for the cross-shaped cross section. These vortices cause higher mixing between the ambient air and the jet, so that more secondary air is induced and the velocity above the opening increases (Fig. 11). The fact that the induced velocities for the elliptic geometry are however lower than for the circular one implies, that the jet's speed is the more important parameter regarding the induction. The cross-shaped geometry combines a high core speed and an enhanced vorticity, which is beneficial for the investigated case. The elliptic geometry suffers of the lower core speed at this plane.

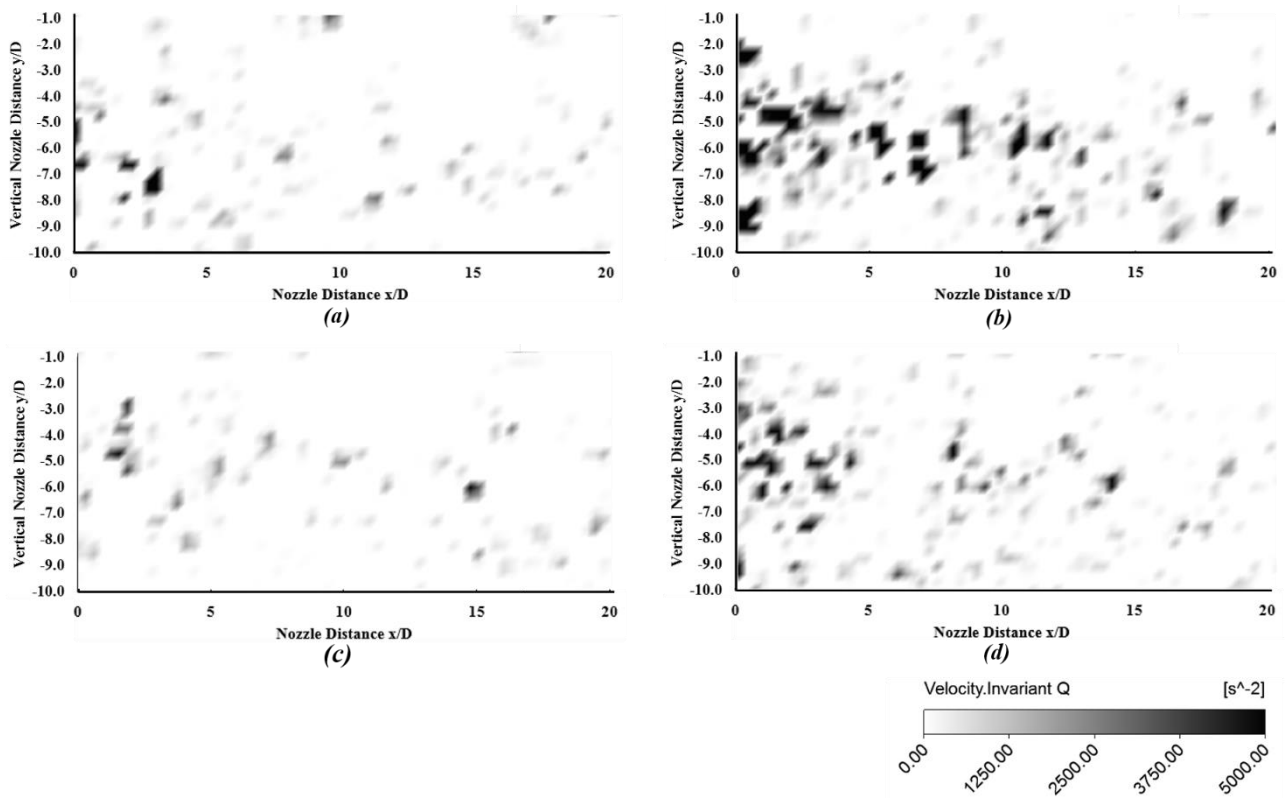

Fig. 12. Q-criterion for circular (a), cross-shaped (b), rectangular (c) and elliptic (d) nozzle cross section

Looking at the $z/D = 0.5$ plane, where the circular jet speed is already heavily decreased, the elliptic jet induces higher flow velocities than for the circular cross section (Fig. 13). This is in good agreement with the earlier explained, wider velocity fields and enhanced vorticity.

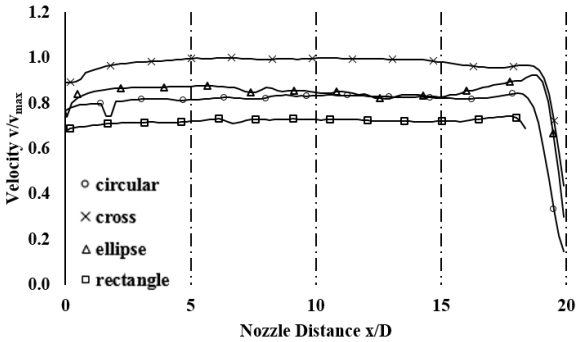

Fig. 13. Velocity profile *v* at *z/D*=0.5 for all geometries

Another parameter that can be taken into account is the inducing area of the jet, e.g. the surface of the jet on which the shear layer develops. As the jet mixes with the ambient air and widens up, the inducing area inside the duct is difficult to determine. To compare the different geometries, only the perimeter of each nozzle cross section is considered in Table 2. The actual inducing area depends on the position inside the duct (x/D). In contrast to the induction ratios in Table 1, the rectangular cross section has the largest perimeter and thus the largest turbulence producing shear layer. This is contradictory to the low produced vorticity shown in Fig. 12. Looking at the other geometries, the increased perimeter results in an increased vorticity. The elliptic perimeter is larger compared to the circular cross section and the cross-shaped cross section is superior to both of them. The result is a larger turbulence producing shear layer, which is confirmed by the higher vorticity shown in Fig. 12. To explain the low vorticity produced by the rectangular cross section, the actual shear layer inside the duct needs to be considered. The velocity profile shown in Fig. 8 indicates that the rectangular shape of the entering air jet collapse immediately inside the duct. So the actual perimeter of the jet is lower compared to the nozzle cross section. Nevertheless, the other jet geometries indicate that an increased perimeter leads to higher vorticity production inside the duct for a stable jet geometry.

Table 2. Perimeter of the different cross sections

	Perimeter [mm]
circular	25.1
cross-shaped	27.7
rectangular	30.1
elliptic	26.1

4 Conclusion and outlook

The findings of this study show that a circular nozzle cross section as it is commonly used today is a good but improvable choice in terms of high IR. A cross-shaped nozzle produces a wider flow field and enhances the vorticity, while maintaining the jet speed. It does also not create higher pressure losses and has no disadvantages when it comes to manufacturing. The other investigated geometries are not as promising as the cross-shaped. The elliptic nozzle also widens up the flow field and enhances the vorticity, because of a larger inducing area of the jet. Compared to the circular jet it suffers of lower core speeds. Nevertheless, it should be further investigated because of the wider flow field and the enhanced vorticity. In the studies of Meslem et al. [7] an aspect ratio of $a/b = 3$ is suggested for the ellipse. Because of manufacturing issues the elliptic cross section in this study is limited to an aspect ratio of $a/b = 1.6$. By using laser cutting, the aspect ratio will not be limited in the future researches. Only the rectangular cross section can be neglected in further researches as it shows no improvement of the flow field or IR. The core speed is low compared to the other cross sections and due to the low inducing area after entering the duct, the vorticity cannot be enhanced. The promising results achieved with the cross-shaped nozzle encourage to also investigate a lobed nozzle, in order to further increase the inducing area. It is also necessary to investigate the interaction of the new nozzle geometries, as they are installed in a row of interacting jets inside an ACB. Another parameter that needs to be taken into account is the acoustic emission of the created flow field, as the acoustic comfort is one major part of indoor applications.

Acknowledgement

Grateful acknowledgement is made for financial support by BMWi (German Federal Ministry of Economics and Technology), promotional reference 03ET1502A.

References

1. P. Mathis, J. Panašková, M. Schmidt, D. Mueller, Roomvent 2014 – 13th SCANVAC international conference on air distribution in rooms pp. 487-495
2. Z. Guan, C.Wen, IEEE 9th Conference on Industrial Electronics and Applications (ICIEA, 2014)
3. H. Freitag, P. Mathis, D. Mueller, CLIMA 2016 – proceedings of the 12th REHVA World Congress: volume **5**
4. W. R. Quinn, AIAA Journal Vol.**32**, No. 3 (1994)
5. K. B. M. Q. Zaman, 34th Aerospace Sciences Meeting and Exhibit (AIAA, 1996)
6. A. Meslem, I. Nastase, F. Allard, *Building and Environment* **12**, 2679-2688 (2010)
7. I. Nastase, A. Meslem, Exp Fluids **4**, 693-714 (2010)
8. ANSYS, Inc. (2016). ANSYS CFX-Solver Modeling/Theory Guide – Release 17.0. ANSYS, Inc.